

# Force distributions in 3D granular assemblies: Effects of packing order and inter-particle friction

Daniel L. Blair, Nathan W. Mueggenburg, Adam H. Marshall, Heinrich M. Jaeger, Sidney R. Nagel

*The James Franck Institute and Department of Physics*

*The University of Chicago*

*5640 S. Ellis Ave. Chicago, IL 60637*

(Received 20 September 2000)

We present a systematic investigation of the distribution of normal forces at the boundaries of static packings of spheres. A new method for the efficient construction of large hexagonal-close-packed crystals is introduced and used to study the effect of spatial ordering on the distribution of forces. Under uniaxial compression we find that the form for the probability distribution of normal forces between particles does not depend strongly on crystallinity or inter-particle friction. In all cases the distribution decays exponentially at large forces and shows a plateau or possibly a small peak near the average force but does not tend to zero at small forces.

PACS numbers: 81.05.Rm, 45.70.-n, 83.70.Fn, 45.70.Cc

## I. INTRODUCTION

In ordinary solids and confined fluids, uniformly applied loads are distributed homogeneously throughout the material. This is not the case for granular materials, which are collections of discrete non-cohesive macroscopic particles [1]. For such systems, stresses are distributed in a highly inhomogeneous manner, along networks containing the largest inter-particle forces [2–6]. These “force chains” support most of the external load, effectively shielding large regions of the material. The probability distribution,  $P(F)$ , of normal forces,  $F$ , between neighboring particles provides a quantitative way of analyzing these stresses [6].  $P(F)$  in granular media exhibits characteristic differences from what would be expected for ordinary solids or fluids.

Recent experiments have measured  $P(F)$  at the container boundaries of granular media [6–10]. When the applied loads are small enough not to cause significant particle deformations two key features of  $P(F)$  have emerged: first,  $P(F)$  exhibits an abundance of small force values, even far below the mean force,  $\bar{F}$ ; and second, for forces above  $\bar{F}$ ,  $P(F)$  decays with a characteristic, exponential dependence. This unusual shape of  $P(F)$  has wide-ranging implications. Compared to a Gaussian profile, the exponential tail indicates a significantly higher probability of an individual contact force greatly exceeding the mean force. In applications with a fixed yield strength, this corresponds to higher chances for material failure. Perhaps even more intriguing is the non-zero value for  $P(F)$  as  $F$  approaches zero. Investigations concerning the structure of force chains have suggested that this abundance of low forces could be caused by arching effects [11–14]. The shape of  $P(F)$  at low forces has also been associated with glassy behavior [15].

As far as the precise functional form for  $P(F)$  is concerned, however, there is currently no clear consensus. Several fitting forms have been proposed, which differ

most widely in their predictions for  $P(F)$  at low forces, ranging from  $P(F) \rightarrow 0$  [16] to  $P(F) \rightarrow \infty$  [11,17,18] as  $F$  approaches zero. Because of the obvious discrepancies not only among some of these model predictions, but also between certain model predictions and the available experimental data, it is important to test the robustness of the results with regard to variations in the bead parameters, the packing construction, and the loading conditions. Experimentally, the issue of whether  $P(F)$  depends on inter-particle friction in any significant way and whether disordered packings behave differently from highly ordered, crystalline configurations has not been tested. Clearly, a perfect, infinite crystal composed of identical grains would result in a delta function for  $P(F)$  since all contact forces are the same in this case. However, it is unknown how the shape of  $P(F)$  is modified by the small amounts of disorder present in real granular crystals. Also it is not known how inter-particle friction influences the distribution of forces.

Here we address these issues with a systematic experimental investigation of the effects on  $P(F)$  of packing order as well as inter-particle friction. Our results confirm the robust character of the probability distribution of forces. We find that  $P(F)$  is essentially independent of changes in the particle arrangement from amorphous to crystalline and changes in the particle surface from smooth to rough. In particular, we observe an exponential decay over more than 2.5 decades for forces larger than the mean. Below the mean force, our data are consistent with either a flat distribution or a small peak centered close to  $\bar{F}$ .

The paper is organized as follows. After a review of currently available theoretical model predictions and simulation results, we introduce our experimental methods, including details of the carbon paper technique used to measure normal forces and a discussion of the experimental uncertainties. We then present results for  $P(F)$  obtained from crystalline and amorphous granular packings using both smooth and rough beads. We also show

how  $P(F)$  evolves with system depth. A final section discusses these results in light of recent experimental and theoretical work on granular and other jammed systems.

## II. BACKGROUND

The original  $q$ -model, proposed by Coppersmith *et al.* [6,16] captures the dominant behavior of  $P(F)$  at large  $F$ :  $P(F/\bar{F}) \propto \exp(-dF/\bar{F})$ , where  $d$  is a positive constant. This model was extended by Nguyen and Coppersmith [19] and by Socolar and Sexton [20,21], and Claudin *et al.* have related it to a diffusion equation with an additional randomly varying convection term [22]. Despite this success, these models predict power-law behavior for  $P(F)$  at forces below the mean force, implying  $P(F) \rightarrow 0$  as  $F \rightarrow 0$ , which disagrees with experimental findings [7,8]. Using contact dynamics computer simulations, Radjai *et al.* [17,18,23] have measured  $P(F)$  and fit it with a slowly diverging power law below  $\bar{F}$  and with a decaying exponential at large forces. This form is qualitatively more consistent with experimental results [7,8].

Recently, the effects of particle deformations on the structure of force chains has been considered. Simulations by Makse *et al.* [9] show evidence for a crossover in the shape of  $P(F)$  from pure exponential to Gaussian as the applied load is increased. However, experiments by Løvoll *et al.* [8] with no external force do not show pure exponential behavior; rather, they are more consistent with the results of Mueth *et al.* [7] at higher deformations. This is in agreement with simulations by Thornton [24,25] and Nguyen and Coppersmith [26], which observe a slow trend toward Gaussian behavior at very large deformations with no evidence of a pure exponential in the low-deformation regime.

Tkachenko and Witten have argued that frictional forces lead to elastic behavior [27]. Simulations performed by Eloy and Clement [28] and by Thornton [29] predict a dependence of  $P(F)$  on inter-particle friction, but this has yet to be seen in experiment.

$P(F)$  has also been studied in simulations of supercooled liquids and glasses [15]. For a liquid with a strongly repulsive core the tail of  $P(F)$  is a decaying exponential at all temperatures. As the temperature of the liquid is lowered to the glass transition,  $P(F)$  develops a small peak centered at  $\bar{F}$  and is very reminiscent of the experimental data on granular systems found by Mueth *et al.* [7].

## III. EXPERIMENTAL METHODS

We have performed experiments on five different granular systems. In order to compare our results with the earlier work of Mueth *et al.* [7], we first examined an amorphous pack of smooth spherical glass beads. We then constructed both hexagonal-close-packed (HCP),

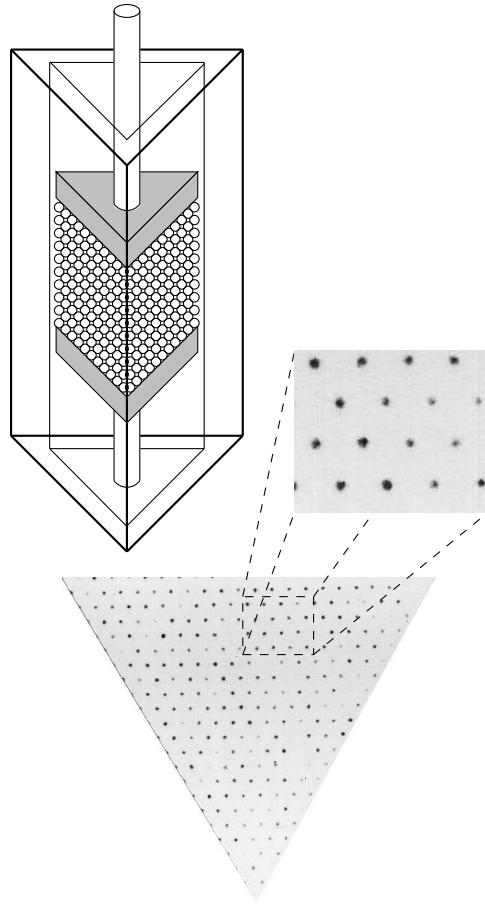


FIG. 1. A schematic of the triangular cell used to contain both crystalline and amorphous packs. A force of 7600 N was applied to the rigidly constrained shaft on the top piston. The cell is 53 bead diameters on a side. A portion of a scanned image of the imprints left on the white paper by a crystal pack is shown with a close-up highlighting the crystalline order.

and face-centered-cubic (FCC) crystalline lattices of the spheres and repeated the experiment on these highly ordered systems. In addition, we examined both amorphous and HCP arrangements of spheres with roughened surfaces.

The experiments were performed using approximately 70,000 soda lime glass spheres with diameter  $3.06 \pm 0.04$  mm. We used an acrylic container of equilateral triangular cross section with a side length of 165 mm, which is commensurate with our HCP crystals (See Fig. 1). The top and bottom boundaries of the system were thick, close-fitting acrylic pistons. The height in layers,  $h$ , of the HCP crystals ranged from 1 to 61, with the bulk of the data being taken at  $h = 45$ . FCC crystals were studied with  $h = 10$ . The amorphous arrangements had a filling height of 12 cm, which corresponds to approximately the same number of particles as in the 45-layer crystals.

## A. Crystal Packing

It is difficult to construct three-dimensional macroscopic crystals of granular materials. Vibration methods for crystallization can efficiently produce triangular close-packed layers [30]; however these methods do not control the stacking order of the planes which is necessary for three-dimensional crystal structures. Also, these methods typically result in large numbers of defects (approximately 10%) which can ruin long range order. We have developed a method to construct near-perfect crystals of glass spheres in an efficient manner. Our technique consists of four steps. First, one layer's worth of beads is placed upon a perforated metal sheet which has small holes arranged in a triangular lattice with a spacing equal to the bead diameter. The array of holes, and therefore the collection of beads, is commensurate with our cell. Second, a vacuum is established behind the perforated plate; this holds the beads in place while the plate is manipulated. Third, the arrangement is inverted and lowered into the cell, which has been precisely machined to accept a monolayer of crystallized beads. The vacuum is then removed to release the beads. Fourth, a small number of residual defects and grain boundaries are removed by hand before the process is repeated to add successive layers. By carefully monitoring the layer-to-layer structure, we were able to create large, nearly perfect HCP structures of arbitrary height with 1,431 and 1,378 particles in alternating layers. Upon construction, each 45-layer HCP crystal contained 70,119 beads with fewer than 10 beads significantly out of place, and typically these defects were confined to the edges of the container.

HCP packings of rough spheres were created in the same manner. Unfortunately, the etching process reduced the bead size by a few micrometers, causing a noticeable incommensurability between the bead lattice and the cell. This resulted in a larger number of defects and less stability.

We also constructed a FCC crystal, but boundary effects made the procedure considerably more difficult. These effects were minimized by rotating the orientation of the pack by thirty degrees. A seed layer was used at the bottom of the cell to arrange the pack in this awkward position. The resulting packing was incommensurate with our cell and was highly unstable; for this reason only one small ( $h = 10$ ) smooth FCC crystal was created.

## B. Rough Particles

Force chains are present only when grains are in contact. This suggests that the highly nonlinear frictional forces between particles may play an important role in determining the network of force chains. To understand the magnitude of these effects on  $P(F)$ , we have varied  $\mu$ , the coefficient of static friction between grains.

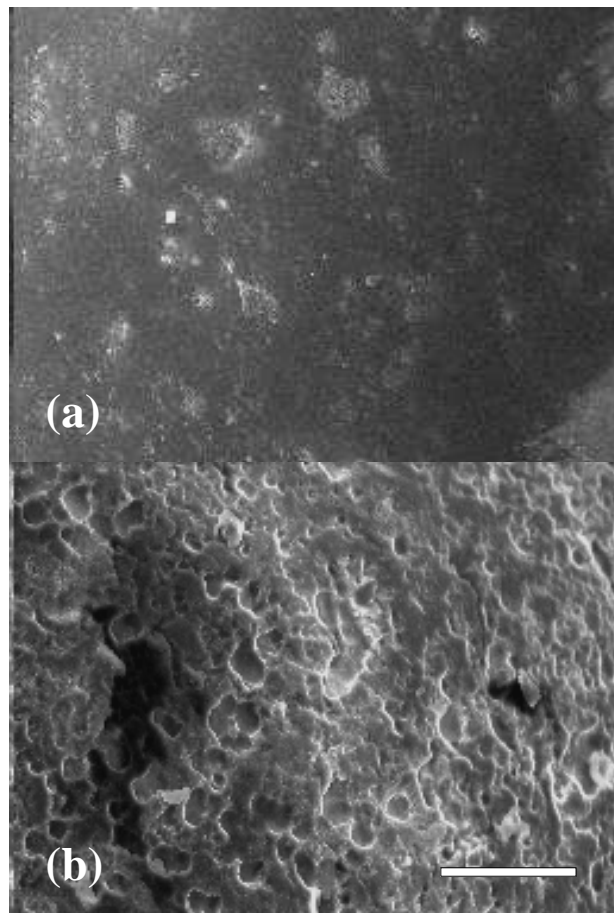


FIG. 2. Scanning electron microscope images of a) a smooth glass bead and b) a glass bead after etching in hydrofluoric acid. The white bar is  $100\ \mu\text{m}$  in length.

A collection of glass spheres was etched in a hydrofluoric acid solution (Ashland Chemical Inc. 7:1 Buffered Oxide Etch) for approximately 2 hours. The difference between the smooth beads and the etched beads was quite apparent by visual inspection. Figure 2 shows scanning electron microscope images of smooth and etched beads. We have quantified the increase in surface friction between grains due to etching using the apparatus shown schematically in Figure 3. The ratio of the coefficients of static friction is characterized by the changes in spring length given by

$$\frac{\mu_{\text{rough}}}{\mu_{\text{smooth}}} = \frac{\Delta x_{\text{rough}} - \Delta x_{\text{sled}}}{\Delta x_{\text{smooth}} - \Delta x_{\text{sled}}} \quad (1)$$

where the change in spring length,  $\Delta x$ , is measured at the point of bead movement, and  $\Delta x_{\text{sled}}$  is included to remove the contribution from friction of the sled with the base. The measured ratio was  $3.0 \pm 0.3$ .

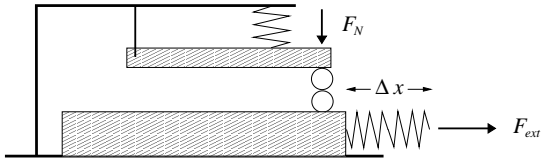


FIG. 3. Schematic of the apparatus for measuring static friction between two beads.  $F_N$  is the normal force applied to the beads, and  $\Delta x$  denotes the spring elongation required to move the bottom bead which is attached to a low-friction sled.

### C. Analysis Techniques for Measuring Local Forces

The experiments were performed as follows. An external force of 7600 N was applied to the top piston of the cell with a pneumatic press, while the bottom piston rested upon a fixed floor. Some force was carried by the walls of the cell, but we determined that this was typically less than 10% of the applied force. We measured the normal forces at the upper and lower boundaries by placing carbon paper and white paper between the granular material and the pistons [31]. This allowed each grain at the boundaries to press into the paper, leaving a mark whose size and intensity were dependent upon the normal force on that bead [6,7,32]. A portion of a scanned image of the resulting imprints is shown in Figure 1. Roughly 2000 marks from both the top and bottom boundaries were identified for each data run. We observed no significant deviations from circular marks, as might be produced by tangential forces.

After each data run, each sheet of white paper was carefully removed and digitized with a flat bed scanner. These digital images were then processed using image analysis software to find both the area and the intensity of each mark. The force on each bead was extracted from the area and intensity of the corresponding feature using calibration curves taken over the same force range. To account for variations in the applied load from run to run, the forces on the individual beads were divided by the average force for each data run. A histogram of the rescaled forces was then averaged over typically 10-20 independent data runs and normalized in order to represent the probability distribution of forces,  $P(f)$ , where  $f \equiv F/\bar{F}$ .

Calibration data were obtained by lowering a known mass connected to a single bead onto carbon paper covering white paper. This system, described in reference [7], consisted of a vertical slide with impulse-absorbing springs; a pulley and cable system was added to ensure that the bead was lowered slowly and monotonically in order to further eliminate impulse forces. Because of the potential variability in carbon paper, each package of paper was calibrated independently. To interpolate a calibration curve from the discrete set of calibration points we used two procedures: 1) a global fourth-order polynomial fit and 2) a local sliding parabolic fit

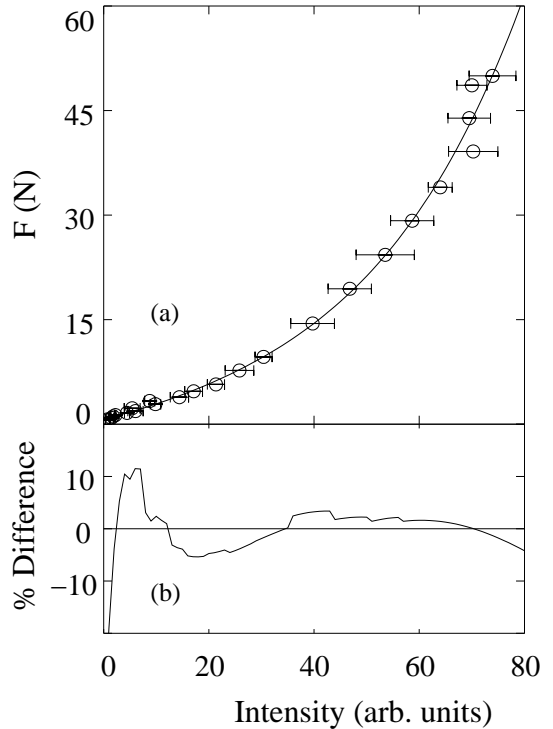


FIG. 4. Calibration data. a) A typical calibration set fit to a global fourth-order polynomial (GFP). b) Percent difference between the fit in the top panel and a local sliding parabolic fit (LSP) to the same data, given by  $100(\text{LSP} - \text{GFP})/\text{GFP}$ . While both interpolations fit the data reasonably well, the differences below the mean force ( $\bar{F} \approx 7\text{N}$ ) shown in the bottom panel can result in large changes to the calculated probability distribution.

with a window of eleven data points. Figure 4a shows a representative set of calibration data together with the fitted fourth-order polynomial. The relationship between force and intensity is monotonic but nonlinear. We found that the force distributions were very sensitive to the calibrations, especially in the low-force regime.

### D. Systematic and Statistical Errors

The uncertainties due to the calibrations are an inherent characteristic of the carbon paper method and represent the largest contribution to systematic errors. The most significant problem is the proper interpolation between calibration points. As shown in figure 4b, the two interpolation methods can lead to significant differences in the intensity-to-force conversion. It is not clear which of the two fitting methods gives the more accurate calibrations, although we found the fourth order polynomial to produce smoother data. For the data shown below, we computed  $P(f)$  using both methods (see insets of figures 5 and 6), and we interpret the difference as an estimate of the systematic error introduced by the calibration.

An additional complication arises from the presence of forces below our threshold of detectability, which is approximately 0.7N. It is difficult to distinguish between undetectably small forces and missing bead contacts, but the number of forces below threshold can be estimated experimentally using the two-sided tape technique described by Mueth *et al.* [7]. An approximate number of very small forces was inserted into the force distributions to account for these undetectable contacts. Errors in the number of undetectable forces affect the normalization and thus effectively rescale  $f$ . Including this source of error, we estimate the uncertainty in the exponential slope to be approximately 5%.

#### IV. RESULTS

We assembled a large number of amorphous and crystalline packs of both smooth and rough glass beads and studied them with the carbon paper technique. As detailed below, the force distributions exhibit exponential behavior for  $f > 1$ . This result has been found previously in experiment, theory, and simulation [7,15,16,23]. Our data are consistent with a small peak in  $P(f)$  near the mean force or with a plateau below the mean force. We found that the force distributions,  $P(f)$ , were well represented in all cases by the functional form

$$P(f) = a(1 - be^{-cf^2})e^{-df} \quad (2)$$

which is a slight generalization of that proposed by Mueth *et al.* [7].

Data was taken at both the top and bottom boundaries of the pack. Very little force was carried by the walls, so that the total force at the bottom, as measured from the carbon dots, was typically within 15% of the force at the top. As had been found previously [7],  $P(f)$  was equivalent between the two surfaces, and the following data represent an average of the results at the top and bottom in order to improve the statistics.

The total forces on both boundaries were typically within 15% of the applied force. This result implies that the carbon marks were dominated by normal forces, as additional tangential forces would have increased the total force. The equivalence between total measured force and applied force also suggests that there were not a significant number of duplicate marks resulting from bead movement as these would also tend to raise the measured total force.

##### A. $P(f)$ : Amorphous vs. Crystalline

Amorphous packs were recreated before each run, which ensured that each run was independent of the others. Figure 5a shows  $P(f)$  for smooth amorphous packs which have been calibrated using the polynomial method.

The data shown represent an average over 32 independent packings. Each run gave approximately 1800 force measurements. The distribution agrees well with that reported by Mueth *et al.* [7]. The solid line in the figure is a fit to Equation 2; the fitting parameters are shown in Table I. The error bars represent the statistical error for multiple data sets, and the insets show  $P(f)$  for low forces calculated using both calibration interpolation methods. We also measured the correlations between pairs of normal forces, and we found no significant correlations for amorphous arrangements.

$P(f)$  for multiple HCP crystals,  $h = 45$ , of smooth beads is shown in figure 5b. This represents an average over 26 runs, distributed over three different HCP crystals with each run giving approximately 2200 force measurements. These data show a similar form to that of the amorphous packs, but there appears to be a slightly higher peak in the smooth crystal data for forces near the average value,  $f \approx 1$ , as well as a slightly steeper exponential decay at large  $f$ . We have seen some evidence of aging (a gradual settling of the grains into a more jammed state) for a single HCP crystal which had been previously subjected to more than 40 runs. We have excluded these data from our results.

To test the robust nature of the probability distribution, we constructed an FCC crystal with  $h = 10$ . Figure 5c shows  $P(f)$  to be virtually indistinguishable from that obtained for the HCP crystal. Due to the difficulties of constructing a crystal incommensurate with our cell, only one FCC crystal was created. The data represent an average of 10 runs with approximately 2000 force measurements each.

##### B. $P(f)$ : Smooth vs. Rough

Amorphous and HCP crystalline packs created with the roughened beads were also studied. The rough amorphous data were taken from 20 independent packings, each representing approximately 1800 force measurements. The rough HCP crystal data were taken from 10 data runs on one crystal with approximately 2200 force measurements each. The resulting force distributions for the rough beads (Fig. 6) were not significantly different from the distributions for the smooth beads (Fig. 5). The fitting coefficients are given in Table I.

All systems, consisting of both smooth and rough beads in both amorphous and crystal packs, showed similar force distributions. The  $P(f)$  curves for four systems are shown together in Figure 7.

##### C. $P(f)$ : Height Dependence

The aforementioned experimental results were obtained for HCP crystals and amorphous packs which were

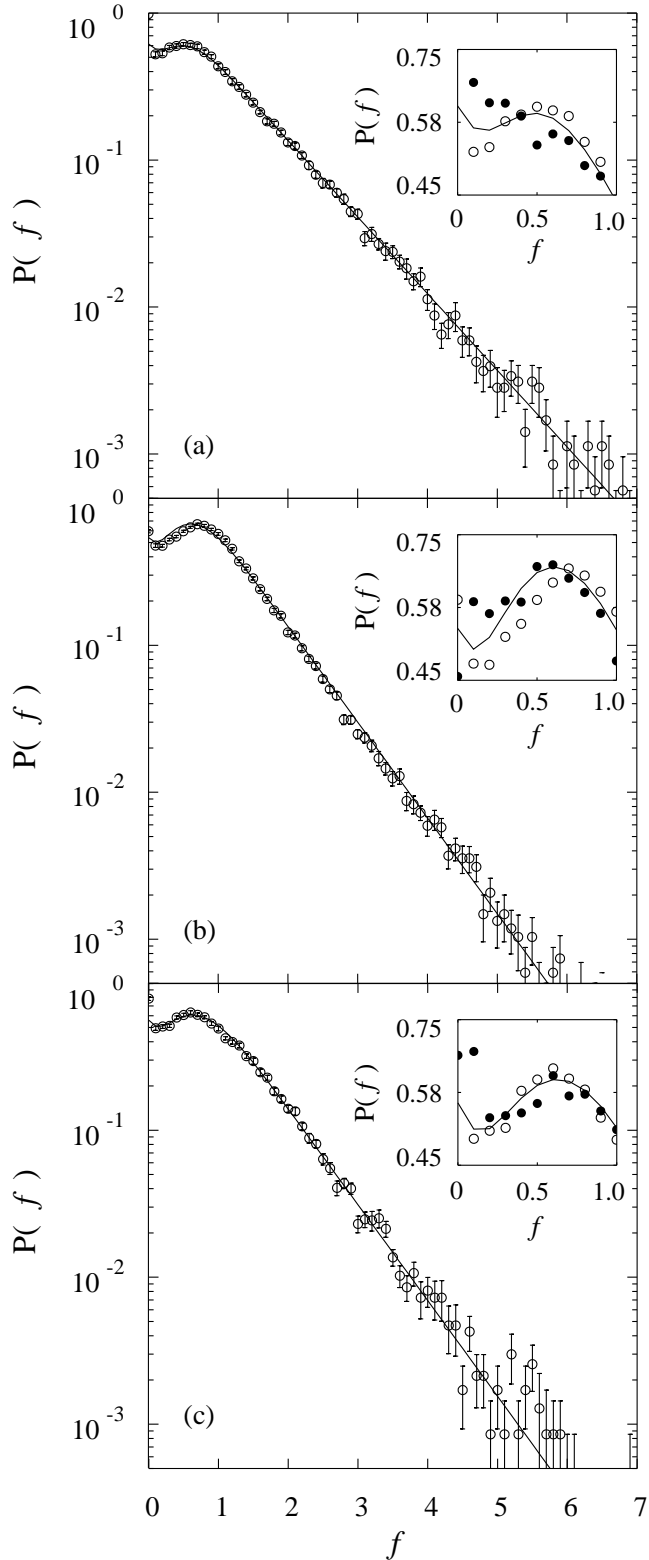


FIG. 5.  $P(f)$  for a) amorphous packs of smooth glass spheres, b) HCP crystalline packs,  $h = 45$ , of smooth glass spheres, and c) an FCC crystalline pack,  $h = 10$ , of smooth glass spheres. The error bars represent the statistical uncertainty, and the solid line represents a fit to Eq. 2. Insets show the difference between the fourth-order polynomial ( $\circ$ ) and sliding parabolic ( $\bullet$ ) interpolation methods.

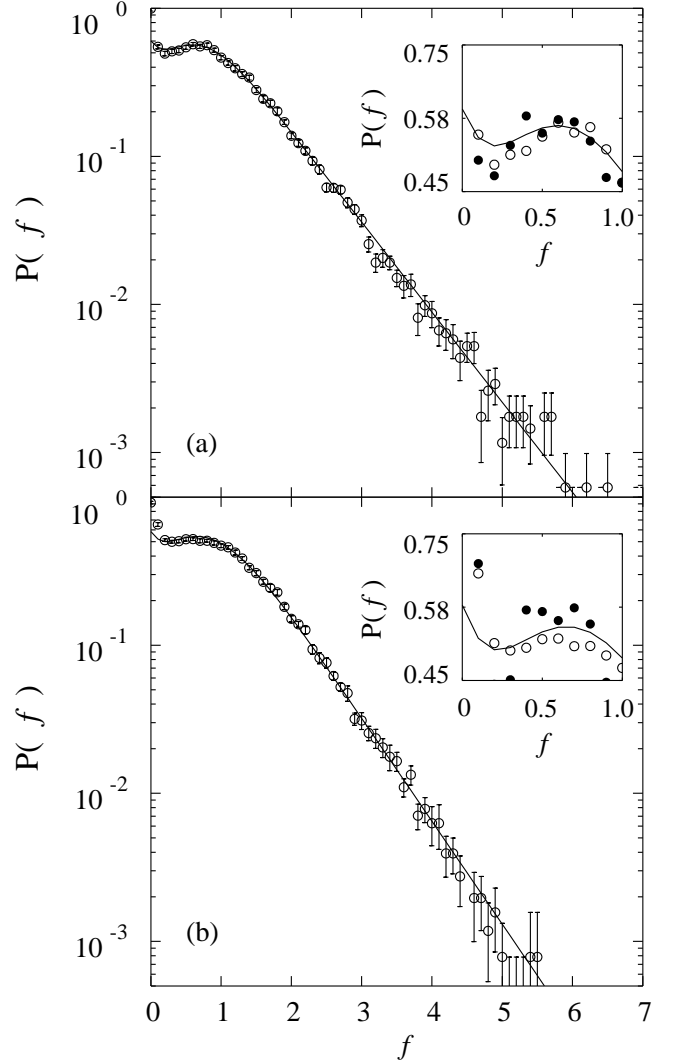


FIG. 6.  $P(f)$  for a) amorphous packs of rough glass spheres and b) HCP crystalline packs,  $h = 45$ , of rough glass spheres. The error bars represent the statistical uncertainty, and the solid line represents a fit to Eq. 2. Insets show the difference between the fourth-order polynomial ( $\circ$ ) and sliding parabolic ( $\bullet$ ) interpolation methods.

Fitting Parameters	$a$	$b$	$c$	$d$
Smooth Amorphous	1.5	0.59	3.1	1.21
Smooth HCP Crystal	2.7	0.80	2.0	1.50
Smooth FCC Crystal	2.8	0.80	1.5	1.48
Rough Amorphous	2.4	0.75	1.4	1.41
Rough HCP Crystal	3.9	0.85	0.8	1.60

TABLE I. Values of fit parameters for the form  $P(f) = a[1 - b \exp(-cf^2)] \exp(-df)$

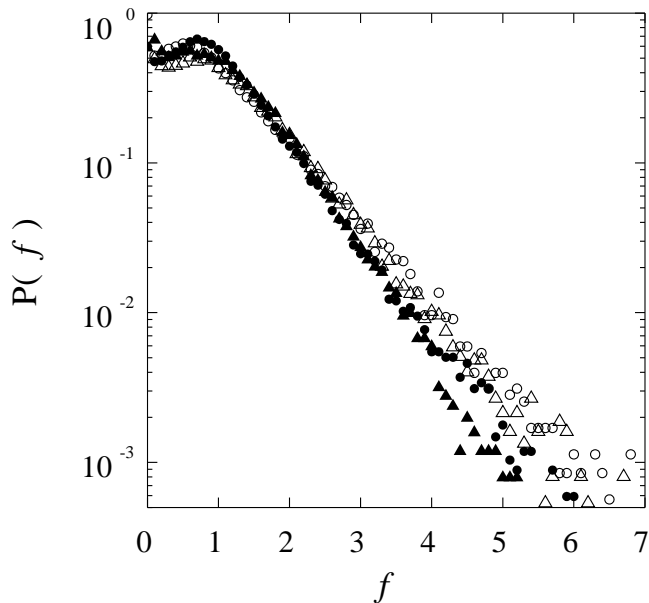


FIG. 7. Force distributions for smooth amorphous ( $\circ$ ), smooth HCP ( $\bullet$ ), rough amorphous ( $\triangle$ ), and rough HCP ( $\blacktriangle$ ) granular packs.

many bead diameters in height. We are interested in understanding how the  $P(f)$  distributions are built up as the height is increased. We studied this question by varying the number of layers in HCP crystals of smooth glass beads. Figure 8 shows  $P(f)$  for HCP crystals of different heights ranging from  $h = 1$  to  $h = 61$ . For comparison, the solid line in each panel represents the fit to Equation 2 for the  $h = 45$  smooth HCP crystals. For a single layer,  $h = 1$ ,  $P(f)$  is determined primarily by the polydispersity of the beads themselves. As the height is increased,  $P(f)$  evolves toward a height-independent form. We find that  $P(f)$  is robust for pack heights greater than  $h \approx 15$ .

#### D. Particle Deformation

Recent simulations on both 2-D and 3-D bead packs suggest that the form of  $P(f)$  depends on particle deformations [9,24–26]. We calculate particle deformations using a Hertzian deformation law [33]:

$$\frac{\delta R}{R} = \left( \frac{2D^2 \bar{F}^2}{R^4} \right)^{\frac{1}{3}}$$

where  $\bar{F}$  is the mean force per bead, and  $R$  is the bead radius.  $D$  is determined by material properties:

$$D = \frac{3(1 - \sigma^2)}{2E}$$

where  $\sigma$  is Poisson's ratio and  $E$  is Young's modulus. Soda lime glass spheres have  $\sigma = 0.24$  and  $E = 69$  GPa [34]. For the data we have presented,  $R =$

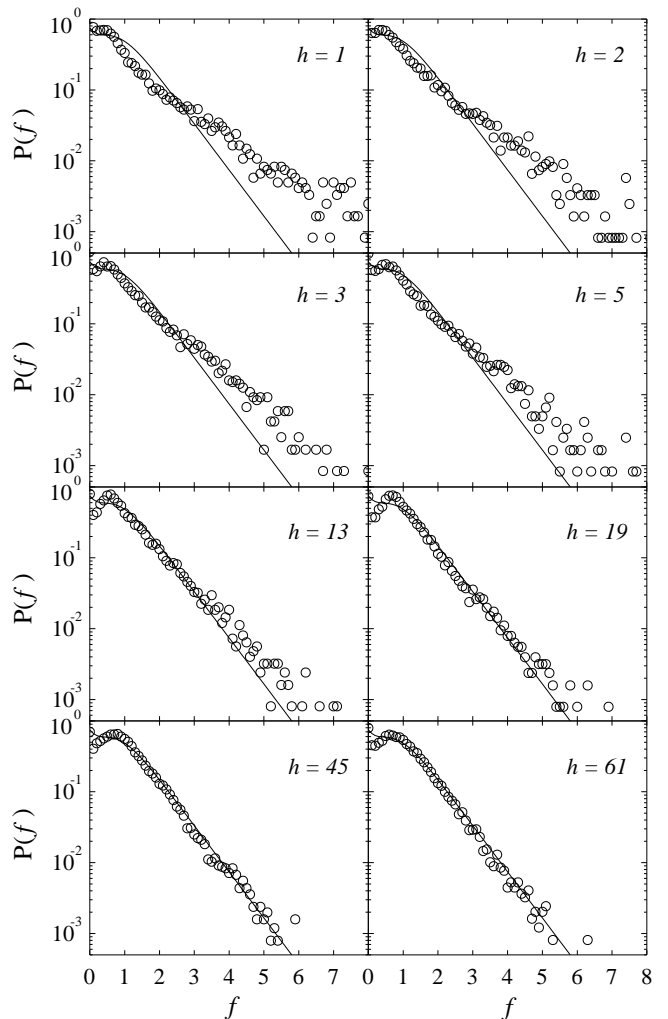


FIG. 8. Force distributions,  $P(f)$ , for smooth HCP crystals of various heights,  $h$ . The solid line is a fit to Eq. 2 for the  $h = 45$  smooth HCP crystal.

1.53 mm, and  $\bar{F} \approx 7.0$  N, resulting in particle deformations of 0.2%. We varied the force applied to the  $h = 45$  HCP crystals over a range of  $\bar{F}$  from 3.5 N to 8.0 N. This corresponded to deformations of 0.12% to 0.2%. Over this limited range, we found that  $P(f)$  remained unchanged.

#### V. DISCUSSION AND CONCLUSIONS

Our data for  $P(f)$  can be well fit by the form given in Equation 2. For forces larger than the mean force, we found  $P(f)$  to be a decaying exponential. For forces smaller than the mean force, our data are consistent with either a small peak or a plateau. There was very little change in the force distribution when the bead pack was varied from amorphous to crystalline, although there is some evidence that the exponential decay for large forces is slightly steeper in the crystalline configurations. There

may also be support for an aging effect, although this is still inconclusive. We found  $P(f)$  to be unaffected when the inter-particle coefficient of friction was changed by a factor of three.

Packing history may also affect the results for an individual data run and could therefore alter the form of  $P(f)$ . A small number of particular runs were found to show significantly different results, such as pure exponential behavior. Only after a considerable number of individual experiments were performed and averaged could a robust probability distribution be presented. We find these variations in the individual runs to be quite surprising. They may indicate that the system is occasionally caught in a state not representative of the average configuration.

We do not see evidence for a change in  $P(f)$  due to the deformation of the particles over a range from 0.12% to 0.2%. Simulations and experiments performed by Makse *et al.* suggest that  $P(f)$  is a pure exponential for small deformations, with a transition to a Gaussian centered at  $f = 1$  when particle deformation is increased [9]. We estimate the deformations to vary from 0.09% to 0.4% in the experiments of Makse *et al.*, while their simulations have a much wider range. The fact that our data do not show a transition toward either pure exponential or Gaussian behavior seems to be in contradiction to their experimental results. Our data are not necessarily inconsistent with their simulations, as our results may be viewed as being in a transition regime between small and large deformations. We note, however, that simulations by Thornton [24,25] as well as Nguyen and Coppersmith [26] find a slow transition toward a Gaussian profile at high deformations (well beyond our range), but do not find a pure exponential in any deformation regime. At low deformations, these simulations show a form of  $P(f)$  which is qualitatively similar to our results. In addition, this form is also consistent with experiments by Løvøll *et al.* [8] on a granular pack with no external forcing and thus very low deformations.

We are able to make qualitative comparisons with the predictions of some theoretical and simulation work for  $P(f)$  in the  $f < 1$  regime. We find that  $P(f)$  does not approach zero as  $f \rightarrow 0$ , in contrast with the predictions of the  $q$ -model [16]. Based on simulations, Radjai *et al.* report a slow power-law divergence as  $f$  approaches zero [17,18,23]; while this form is similar to our experimental results (since the power-law exponent is very small), it does not account for the possibility of a peaked distribution near the mean.

Simulations performed by O'Hern *et al.* [15] on quenched molecular liquids in two dimensions show the most apparent similarities to our results. For potentials with finite repulsive terms, such as a Lennard-Jones potential with a range cut off at its minimum value, the  $P(f)$  distribution is indistinguishable from our findings. Also, there may exist a correlation between granular crystals which have aged (as mentioned above) and quenched molecular liquids at temperatures well below the glass-

transition temperature. The increase of the exponential slope as well as a slight peak near the mean force in crystalline configurations are similar to those found in jammed fluids where large forces cannot relax when quenched below the glass-transition temperature.

## VI. ACKNOWLEDGMENTS

We thank Sue Coppersmith, Qiti Guo, Steve Langer, Andrea Liu, Milica Medved, Corey O'Hern, Raghuvver Parthasarathy, Denise Sawicki, Alexei Tkachenko, Mary Upton, and Tom Witten. We especially thank Dan Mueth for the background on which this work was built as well as his continued interest, comments, and criticisms. This work was supported by NSF under Grant No. CTS-9710991 and by the MRSEC Program of the NSF under Grant No. DMR-9808595.

- 
- [1] H. M. Jaeger, S. R. Nagel, and R. P. Behringer, *Physics Today* **49**, 32 (1996); *Rev. Mod. Phys.* **68**, 1259 (1996).
  - [2] P. Dantu, in *Proceedings of the 4th International Conference On Soil Mechanics and Foundation Engineering* London, 1957 (Butterworths, London, 1958), Vol. 1, pp. 144-148.
  - [3] P. Dantu, *Ann. Ponts Chauss.* **IV**, 193 (1967).
  - [4] D. Howell, R. P. Behringer, in *Powders & Grains 97*, edited by R. P. Behringer and J. T. Jenkins (Balkema, Rotterdam, 1997), pp. 337-340.
  - [5] M. Ammi, D. Bideau, and J. P. Troadec, *J. Phys. D: Appl. Phys.* **20**, 424 (1987).
  - [6] C.-h. Liu, S. R. Nagel, D. A. Schecter, S. N. Coppersmith, S. Majumdar, O. Narayan, and T. A. Witten, *Science* **269**, 513 (1995).
  - [7] D. M. Mueth, H. M. Jaeger, S. R. Nagel, *Phys. Rev. E* **57**, 3164 (1998).
  - [8] G. Løvøll, K. N. Måløy, E. G. Flekkøy, *Phys. Rev. E* **60**, 5872 (1999).
  - [9] H. A. Makse, D. L. Johnson, L. M. Schwartz, *Phys. Rev. Lett.* **84**, 4160 (2000).
  - [10] G. W. Baxter, in *Powders & Grains 97*, edited by R. P. Behringer and J. T. Jenkins (Balkema, Rotterdam, 1997), pp. 345-348.
  - [11] P. Claudin and J.-P. Bouchaud, *Phys. Rev. Lett.* **78**, 231 (1997).
  - [12] S. Luding, *Phys. Rev. E* **55**, 4720 (1997).
  - [13] J. Duran, E. Kolb, and L. Vanel, *Phys. Rev. E* **58**, 805 (1998).
  - [14] R. Peralta-Fabi, C. Málaga, and R. Rechtman, *Europhys. Lett.* **45**, 76 (1999).
  - [15] C. S. O'Hern, S. A. Langer, A. J. Liu, and S. R. Nagel, in press. *cond-mat/0005035*.
  - [16] S. N. Coppersmith, C. Liu, S. Majumdar, O. Narayan, and T. A. Witten, *Phys. Rev. E* **53**, 4673 (1996).
  - [17] F. Radjai, M. Jean, J. J. Moreau, and S. Roux, *Phys. Rev. Lett.* **77**, 274 (1996).



- [18] F. Radjai, D. E. Wolf, S. Roux, M. Jean, and J. J. Moreau, in *Powders & Grains 97*, edited by R. P. Behringer and J. T. Jenkins (Balkema, Rotterdam, 1997), pp. 211-214.
- [19] M. L. Nguyen, and S. N. Coppersmith, *Phys. Rev. E* **59**, 5 (1999).
- [20] J. E. S. Socolar, *Phys. Rev. E* **57**, 3204 (1998).
- [21] M. G. Sexton, J. E. S. Socolar, and D. G. Schaeffer, *Phys. Rev. E* **60**, 1999 (1999).
- [22] P. Claudin, J.-P. Bouchaud, M. E. Cates, and J. P. Wittmer, *Phys. Rev. E* **57**, 4 (1998).
- [23] F. Radjai, D. Wolf, M. Jean, and J. J. Moreau, *Phys. Rev. Lett.* **80**, 61 (1998).
- [24] C. Thornton, *KONA Powder and Particle* **15**, 81 (1997).
- [25] C. Thornton and S. J. Antony, *Phil. Trans. Roy. Soc. A.* **356**, 2763 (1998)
- [26] M. L. Nguyen, and S. N. Coppersmith, in press. *cond-mat/0005023*.
- [27] A. V. Tkachenko, T. W. Witten, *Phys. Rev. E* **60**, 687 (1999).
- [28] C. Eloy and E. Clément, *J. Phys. I France* **7**, 1541 (1997).
- [29] C. Thornton, *Geotechnique* **50**, 43 (2000).
- [30] O. Pouliquen, M. Nicolas, and P. D. Weidman, *Phys. Rev. E* **79**, 3640 (1997).
- [31] We used Super Nu-Kote SNK-11 1/2 carbon paper and Hammermill Laser Print Long Grain Radiant White paper.
- [32] F. Delyon, D. Dufresne, and Y.-E. Lévy, *Ann. Ponts Chauss.* 22 (1990).
- [33] L. Landau and E. Lifshitz, *Theory of Elasticity* (Pergamon, Oxford, 1959), pp. 34-35.
- [34] *CRC Handbook of Tables for Applied Engineering Science*, edited by R. Bolz and G. Tuve, (CRC Press, Boca Raton, 1970), pp. 160-163.